

Multiwall Boron Carbonitride/Carbon Nanotube Junction and Its Rectification Behavior

Lei Liao,^{†,‡} Kaihui Liu,[†] Wenlong Wang,[†] Xuedong Bai,^{*,†} Enge Wang,^{*,†} Yueli Liu,[§] Jinchai Li,[‡] and Chang Liu[‡]

Institute of Physics, Chinese Academy of Sciences, Beijing 100080, China, Department of Physics, Wuhan University, Wuhan 430072, China, and School of Materials Science and Engineering, Wuhan University of Technology, Wuhan, 430070, China

Received April 24, 2007; E-mail: xdbai@aphy.iphy.ac.cn; egwang@aphy.iphy.ac.cn

In recent years, the ternary boron carbonitride (BCN) nanotubes have attracted increasing interests because of their unique electronic properties and potential technological applications. A prime advantage of the BCN nanotubes over their carbon counterparts is the relative simplicity in manipulating the electronic structures. Theoretical calculations have predicted that the band gap of BCN nanotubes can be tailored over a wide range by chemical composition rather than by geometrical structure.^{1–3} The BCN nanotubes could be quite promising in applications for nanoscale electronic and photonic devices.

Many efforts have been devoted to the synthesis of BCN nanotubes since the first report in 1994.⁴ Nanotubes with a homogeneous BCN composition or separated phases of BN and C layers have been prepared by various means of arc discharge, laser ablation, and chemical vapor deposition (CVD).^{5–8} The electrical transport measurements performed on BCN nanotube bundles⁹ and photoluminescence from large-scale BCN nanotube arrays¹⁰ have presented its semiconductor nature. Recently, a band gap of ~ 2.8 eV¹¹ for the $B_{0.45}C_{0.1}N_{0.45}$ nanotube and a band gap of 3.89 eV¹² for the BCN nanotube with $\sim 1:1:1$ stoichiometry have been identified by X-ray photoelectron spectroscopy and cathodoluminescence, respectively. In addition, the BCN nanojunctions have been studied through varying the local chemical composition of the nanotube.^{1a,13} The “tunable” composition of BCN nanotube may provide us with a reliable and economical way to achieve nanotube heterojunctions for rectifying diodes, light emitting diodes, transistors, and so forth.

In this Communication, the direct synthesis of massive BCN/C nanotube junctions has been realized via a bias-assisted hot-filament CVD method. The electrical transport measurements of individual nanotube junctions were carried out on a conductive atomic force microscopy (AFM). It is found that the BCN/C nanotube junctions show a typical rectifying diode behavior.

The BCN/C nanotubes were grown in a hot-filament CVD apparatus, by which the single-wall BCN nanotubes have newly been synthesized.¹⁴ In this study, clean nickel wafers were used as the substrates and a dc power supply was supplied to generate glow discharge plasma between the substrate and the tantalum anode installed above a carbonized tungsten filament. The BCN/C nanotube junctions were synthesized in a continuous CVD process with a two-step growth. First, the flow rates of N_2 , H_2 , and CH_4 were kept at 75, 5, and 20 sccm, respectively. When the filament was heated to about 1600 °C, a bias of 600 V was applied to produce the glow discharge plasma, and the growth started at 2.0 kPa. After growth for 10 min, the temperature of the filament was

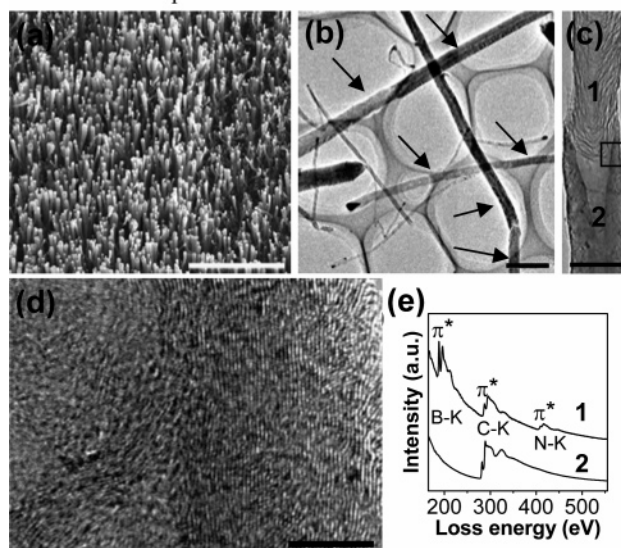


Figure 1. (a) SEM image of the as-grown BCN/C nanotube junction array; scale bar = 5 μ m. (b) TEM image of BCN/C nanotube junctions; scale bar = 200 nm. (c) A single BCN/C nanotube junction; scale bar = 50 nm. (d) High-resolution TEM image from the area marked by rectangle in Figure 1c; scale bar = 5 nm. (e) EELS spectra taken from the section 1 and 2 in panel c, respectively.

rapidly decreased to 1500 °C, and the B_2H_6 gas with a concentration of 5 vol % was introduced into the chamber. In this way, multiwall BCN nanotubes were grown on the top of the carbon nanotubes, and the BCN/C nanotube junctions with sharp interface were formed.

Figure 1a is a typical scanning electron microscopy (SEM) image of the large-scale aligned BCN/C nanotube arrays grown on nickel substrates. The nanotubes are 8–10 μ m in length and 50–150 nm in diameter. A transmission electron microscopy (TEM) image of the as-grown BCN/C nanotubes is shown in Figure 1b, which reveals that most of nanotubes consist of two sections, marked by arrows. From an enlarged TEM image (Figure 1c), the nanotube is composed of two thoroughly different parts, one side is a herringbone-like BCN nanotube while the other is a cylinder-like multiwall carbon nanotube, marked by 1 and 2, respectively. The two parts with different atomic and electronic structures make contact with each other and form a seamless nanotube, seen from high-resolution TEM image, as indicated in Figure 1d (also see Supporting Information, Figure S1). Thus, the BCN/C nanotube junctions are obtained by the sharp interface between the BCN nanotube and the carbon nanotube. Figure 1e shows the electron energy-loss spectroscopy (EELS) spectra taken from the two parts around the junction in Figure 1c, corresponding with the section 1

[†] Institute of Physics, Chinese Academy of Sciences.

[‡] Wuhan University.

[§] Wuhan University of Technology.

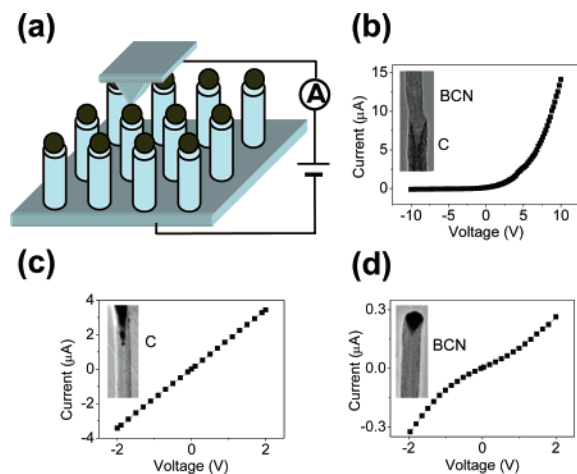


Figure 2. (a) Scheme of the experimental setup for the electrical transport measurement of individual nanotubes by an AFM technique. (b–d) I – V curves for a single BCN/C nanotube junction, carbon nanotube, and BCN nanotube,; the insets of panels b–d schematically showing the corresponding different nanotubes.

and 2, respectively. In the EELS spectrum from part 1 region, K-edges of B, C, and N can be clearly identified. The sharply defined π^* and σ^* fine structure features of the C K-edge are characteristic of sp^2 bonding. The B and N K-edge signals also show a discernible π^* peak as well as a σ^* band, indicating that the B and N atoms are in the same sp^2 -hybridized state as their C counterparts. This means that the B and N atoms are doped into the graphite network by substitution of C atoms, and the local chemical composition $B_{0.25}C_{0.45}N_{0.30}$ is determined quantitatively from EELS data, which is close to BC_2N . While only C signal is observed in the EELS spectrum from the part 2 region, indicating a pure carbon nanotube. The ternary bonding nature of the BCN nanotubes was further confirmed by photoelectron spectroscopy (XPS) characterization, and the BCN/C nanotube junctions were also examined by micro-Raman spectroscopy experiments (see Supporting Information, Figure S2 and S3).

The electrical transport measurements of individual BCN/C nanotube junctions were performed on an AFM with an Au-coated Si tip, as schematically drawn in Figure 2a. The AFM experiment is presented in the Supporting Information. Since the mechanism of the nanotube is top growth,^{8b} the nickel catalyst particle is located on the top of the nanotube, which acts as an electrode of the nanotube to be in contact with the AFM tip, while the nickel substrate acts as the other electrode. The direct top-growth on metal substrates makes nanotubes with good contacts on both ends.

Figure 2b shows a typical current–voltage (I – V) curve of BCN/C nanotube junctions, which are highly nonlinear and asymmetric with a rectification ratio of $\sim 10^3$, resembling that of a rectifying nanodiode with a turn-on voltage at ~ 0.7 V and a reverse bias breakdown voltage at about -12 V. The details of Figure 2b on the same axes regime as that of Figure 2d can be seen in the Supporting Information, Figure S4. The current rectification phenomenon was observed in over 90% of the 120 nanotube junctions studied in our experiments. The high rectification ratio,

low turn-on voltage, and high reverse breakdown voltage indicate that the BCN/C nanotube intramolecular junction has a good rectifying property as a high-performance nanodiode.

For a further understanding of the rectification behavior of BCN/C junctions, the I – V measurements were also carried out on pure carbon nanotubes and BCN nanotubes. The results are shown in Figure 2c and Figure 2d. In both cases, the I – V curves are linear or nearly linear, which is in agreement with their expected intrinsic properties and indicates the contact between nanotube and AFM tip can be ruled out in the rectification behavior. The I – V characteristic of BCN nanotube in Figure 2d also reveals its semiconductor nature. Therefore, we conclude that the rectifying behavior of the BCN/C nanotube is attributed to the intrinsic heterojunction structures. The mechanism for the electronic rectification is discussed in Supporting Information.

In summary, the direct synthesis of massive BCN/C nanotube junctions in a simple way has been presented. The nanotube tip-growth mode and its direct growth on metal substrate make good contact attainable for electrical measurement and for device performance study. The BCN/C nanotube junctions show a typical rectifying diode behavior. It is believed that the BCN/C heterojunction may find a variety of applications in electronic and optoelectronic devices.

Acknowledgment. Financial support from the NSF (Nos. 10510033, 10540420033, 60621091, and 10134030), MOST (No. 2006AA03Z402), and CAS of China is acknowledged.

Supporting Information Available: Experimental methods, XPS, Raman characterizations, and discussion on mechanism of rectification. This material is available free of charge via the Internet at <http://pubs.acs.org>.

References

- (1) (a) Blasé, X.; Charlier, J.-C.; De Vita, A.; Car, R. *Appl. Phys. A* **1999**, *68*, 293. (b) Blasé, X.; Charlier, J.-C.; De Vita, A.; Car, R. *Appl. Phys. Lett.* **1997**, *70*, 197.
- (2) Miyamoto, Y.; Rubio, A.; Cohen, M. L.; Louie, S. G. *Phys. Rev. B* **1994**, *50*, 4976.
- (3) Enyashin, A. M.; Makurin, Y. N.; Ivanovskii, A. L. *Carbon* **2004**, *42*, 2081.
- (4) Stéphane, O.; Ajayan, P. M.; Colliex, C.; Redlich, P.; Lambert, J. M.; Bernier, P.; Lefin, P. *Science* **1994**, *266*, 1683.
- (5) (a) Weng-Sieh, Z.; Cherrey, K.; Chopra, N. G.; Blasé, X.; Miyamoto, Y.; Rubio, A.; Cohn, M. L.; Louie, S. G.; Zettl, A.; Gronsky, A. R. *Phys. Rev. B* **1995**, *51*, 11229. (b) Suenaga, K.; Colliex, C.; Demoncey, N.; Loiseau, A.; Pascard, H.; Willaime, F. *Science* **1997**, *278*, 653.
- (6) Terrones, M.; Grobert, N.; Terrones, N. *Carbon* **2002**, *40*, 1665.
- (7) Zhang, Y.; Gu, H.; Suenaga, K.; Iijima, S. *Chem. Phys. Lett.* **1997**, *279*, 264.
- (8) (a) Ma, R.; Golberg, D.; Bando, Y.; Sasaki, T. *Philos. Trans. R. Soc. London, Ser. A* **2004**, *362*, 216. (b) Bai, X. D.; Guo, J. D.; Yu, J.; Wang, E. G.; Yuan, J.; Zhou, W. Z. *Appl. Phys. Lett.* **2000**, *76*, 2624.
- (9) Terrones, M.; Golberg, D.; Grobert, N.; Seeger, T.; Reyes-Reyes, M.; Mayne, M.; Kamalakaran, R.; Dorozhkin, P.; Dong, Z.-C.; Terrones, H.; Rühle, M.; Bando, Y. *Adv. Mater.* **2003**, *15*, 1899.
- (10) Bai, X. D.; Wang, E. G.; Yu, J.; Yang, H.; *Appl. Phys. Lett.* **2000**, *77*, 67.
- (11) Kim, S. Y.; Park, J.; Choi, H. C.; Ahn, J. P.; Hou, J. Q.; Kang, H. S. *J. Am. Chem. Soc.* **2007**, *129*, 1705.
- (12) Yin, L. W.; Bando, Y.; Golberg, D.; Gloter, A.; Li, M. S.; Yuan, X. L.; Sekiguchi, T.; *J. Am. Chem. Soc.* **2005**, *127*, 16354.
- (13) Guo, J. D.; Zhi, C. Y.; Bai, X. D.; Wang, E. G. *Appl. Phys. Lett.* **2002**, *80*, 124.
- (14) Wang, W. L.; Bai, X. D.; Liu, K. H.; Xu, Z.; Golberg, D.; Bando, Y.; Wang, E. G.; *J. Am. Chem. Soc.* **2006**, *128*, 6530.

JA072861E